ACS OMEGA

Article

Cite This: ACS Omega 2019, 4, 12244−12251

http://pubs.acs.org/journal/acsodf

Melanin: A Greener Route To Enhance Energy Storage under Solar Light

Ri Xu,[†,∥] Abdelaziz Gouda,[†,∥] Maria Federica Caso,[‡] Francesca Soavi,*[,§] and Clara Santato*[,†]

[†]Department of Engineering Physics, Polytechnique Montréal, C.P. 6079, Succursale Centre-ville, Montréal, QC H3C 3A7, Canada

[‡]Nanofaber Spin-Off at ENEA, Casaccia Research Centre, Via Anguillarese 301, Roma 00123, Italy

[§]Dipartimento di Chimica "Giacomo Ciamician", Alma Mater Studiorum Università di Bologna, Via Selmi, 2, 40126 Bologna, Italy

Supporting Information

ABSTRACT: The development of technologies integrating solar energy conversion and energy storage functions is critical for limiting the anthropogenic effects on climate change and preventing possible energy shortages related to the increase of the world population. In our work, we explored the possibility to integrate the conversion and storage functions within the same multifunctional biosourced material. We identified the redox-active, quinone-based, melanin pigment, featuring a broadband absorption in the UV−vis region, as the ideal candidate for such an exploration. Electrodes of melanin on carbon paper were investigated for their morphological, optical, and voltammetric characteristics prior to being assembled into symmetric supercapacitors operating in aqueous electrolytes. We observed that, under solar light, the capacity and capacitance of melanin electrodes significantly increase with respect to the dark conditions (by 22 and 39%, respectively). Once in a supercapacitor configuration, besides featuring a Coulombic efficiency close to 100% after 5000 cycles, the capacitance and capacity of the electrodes, rated by the initial values, improve after prolonged illumination, as it is the case for the energy and power density.

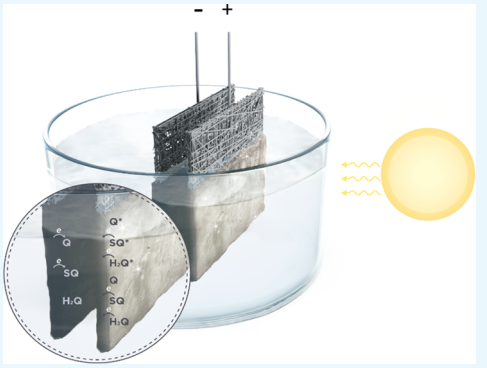

1. INTRODUCTION

The development of sustainable and efficient energy conversion and storage technologies is critical for limiting the anthropogenic effects on climate change and preventing possible energy shortages related to the increase of the world population.[1]

The Sun is the most abundant renewable energy source for our planet. Electrochemical technologies have been widely investigated to store intermittent solar energy, after its conversion into electrical energy by photovoltaic (PV) cells.[2,3] In this regard, the development of technologies integrating solar energy conversion and energy storage functions, aiming at maximizing the efficiency of the solar light utilization, is of utmost importance. Photo-supercapacitors and solar batteries are examples of such integrated technologies.[4] A number of energy conversion/storage integrated structures have been reported in the literature, based on different types of PV (e.g., dye-sensitized, perovskite, and hybrid) and storage devices (e.g., Li-ion batteries, redox flow batteries, and supercapacitors; please refer to the review of the literature reported in Table S1). A promising development is represented by the possibility to integrate the conversion and storage functions within the same multifunctional material. Suitable optical absorption and electrochemical energy storage properties are essential for such a multifunctional material to satisfy the requirements for integrated solutions based on only one photo- and redox-active material. Sustainability, i.e., being abundant, nontoxicity, low cost, biosource, or synthesis along the principles of green chemistry, is another essential requirement for such a material.

Nature is a source of abundant, environmentally benign, carbon-based redox-active materials, capable of absorbing solar energy. Quinone-based molecules are organic redox materials widely studied for electrochemical energy storage.[5−18] Liang et al. exploited polypyrene-4,5,9,10-tetraone as an anode in aqueous Li^+ batteries (pH 7) and obtained a specific capacity of 229 mAh g^{-1}, with 80% capacity retention after 3000 cycles.[12] Sun et al. reported on polydopamine as an electrode and a binder material; capacities as high as 1818 and 500 mAh g^{-1} were reported for Li^+ and Na^+ batteries, respectively.[16] Vonlanthen et al. fabricated polyaniline−benzoquinone−hydroquinone electrodes for supercapacitors with high cycling stability (>50 000 cycles) and high pseudocapacitance (1500 F g^{-1}).[19]

Eumelanin, a quinone-based pigment ubiquitous in flora and fauna, is an attractive candidate to explore the feasibility of integrating energy conversion and storage functions, within the same material. Eumelanin features a number of physicochemical properties, apart from redox activity: UV−vis absorption, photoconductivity, hydration-dependent electrical conductiv-

Received: April 12, 2019
Accepted: July 3, 2019
Published: July 16, 2019

DOI: 10.1021/acsomega.9b01039
ACS Omega 2019, 4, 12244−12251

Scheme 1. Hydroquinone (H2Q), Semiquinone (SQ), and Quinone (Q) Redox Forms of the Building Blocks of Eumelanin: 5,6-Dihydroxyindole (DHI) and 5,6-Dihydroxyindole-2-carboxylic acid (DHICA). R is −H in DHI, whereas R is the −COOH Group in DHICA. The Quinone Imine Form (QI) is the Tautomer of Q

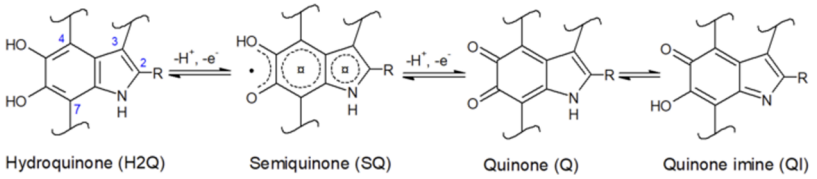

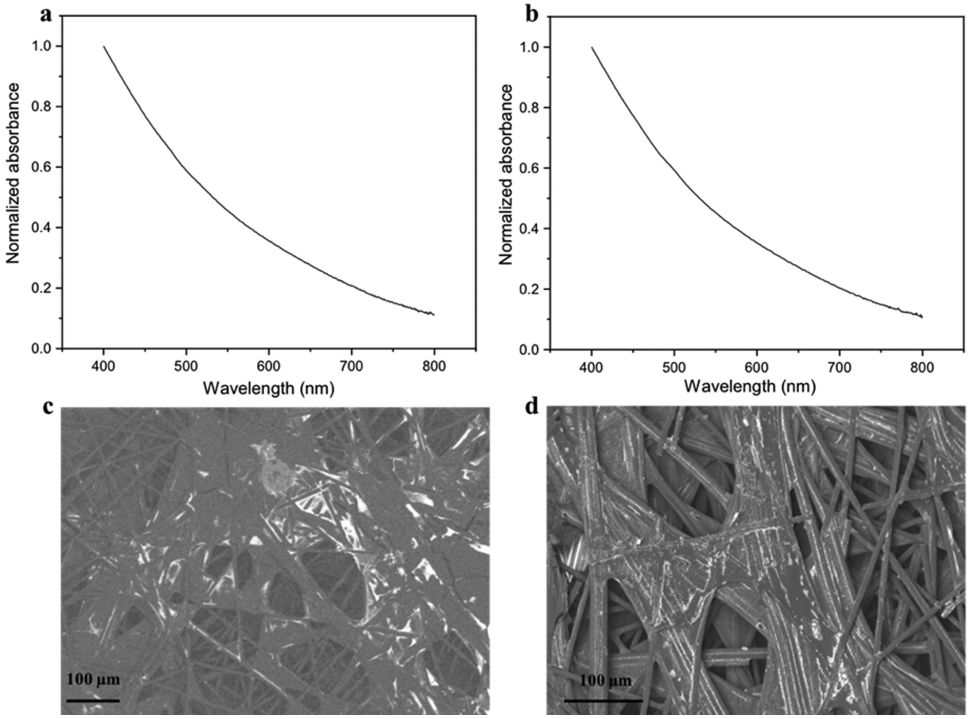

Figure 1. Absorption spectra of (a) DHI-melanin and (b) DHI/DHICA-melanin spin-coated on Corning glass (loading 0.1 mg cm^{-2}). SEM images of (c) DHI-melanin and (d) DHI/DHICA-melanin drop-cast on carbon paper and stained with uranyl acetate, obtained in backscattered electron (BSE) mode, with an accelerating voltage 5 kV. The bright regions correspond to eumelanin chelating uranyl oxycations.[32,33]

ity, metal-binding affinity (chelation), antioxidant, and free radical scavenging.[20−22] Eumelanin is based on 5,6-dihydroxyindole (DHI) and 5,6-dihydroxyindole carboxylic acid (DHICA) building blocks (Scheme 1), coexisting in different redox states. Natural eumelanin (Sepia melanin, extracted from cuttlefish ink) can contain up to 50% DHICA, in molecular ratio.[23] Chemically controlled melanins (DHI-melanin and DHICA-melanin, obtained from the polymerization of only one of the two eumelanin building blocks) are used in the literature to elucidate fundamental aspects of physicochemical processes taking place in melanin. UV−vis spectra of DHICA-melanin feature an absorption peak below 400 nm and a weaker visible-light absorption, compared to those of DHI-melanin.[24] The decreased visible absorption of DHICA-melanin is attributable to the steric hindrance of the carboxyl groups on the DHICA building blocks leading to nonplanar polymer structures that limit electronic delocalization and transport.[24,25]

Eumelanin-based electrodes assembled into supercapacitors and Na^+ batteries operating in aqueous media have been reported in the literature.[7,26] Kumar et al. reported on the use of Sigma melanin as a supercapacitor electrode material (specific capacitance 167 F g^{-1}, specific capacity 24 mAh g^{-1}, and capacitance retention 75% after 1000 cycles).[26] Kim et al. reported on natural and synthetic melanin as cathode (specific capacity of 61.6 mAh g^{-1}) and anode (specific capacity of 16.1 mAh g^{-1}) materials.[7,27] The pigment has also been investigated for photovoltaic applications.[28,29]

The combination of optical and redox properties in the multifunctional eumelanin pigment calls for the exploration of the possibility to enhance the electrochemical energy storage performance of eumelanin-based electrodes under solar light illumination. The superior optical and electrochemical energy storage properties of DHI melanin over the DHICA counterpart[24,25] render DHI-melanin the ideal synthetic candidate to explore the full potential of melanin for integrated conversion and storage technologies. To model the behavior of natural melanin, studies making use of synthetic melanin, obtained from the two building blocks, are pertinent.

In this work, we report on the effect of solar light on the electrochemical energy storage properties of eumelanin electrodes on carbon paper, assembled in supercapacitors operating in aqueous electrolytes. We used chemically controlled melanins, namely, DHI-melanin and DHI/DHICA-melanin (weight/weight 7/3), the latter to model the behavior of natural melanin.[23] Scanning electron

DOI: 10.1021/acsomega.9b01039
ACS Omega 2019, 4, 12244−12251

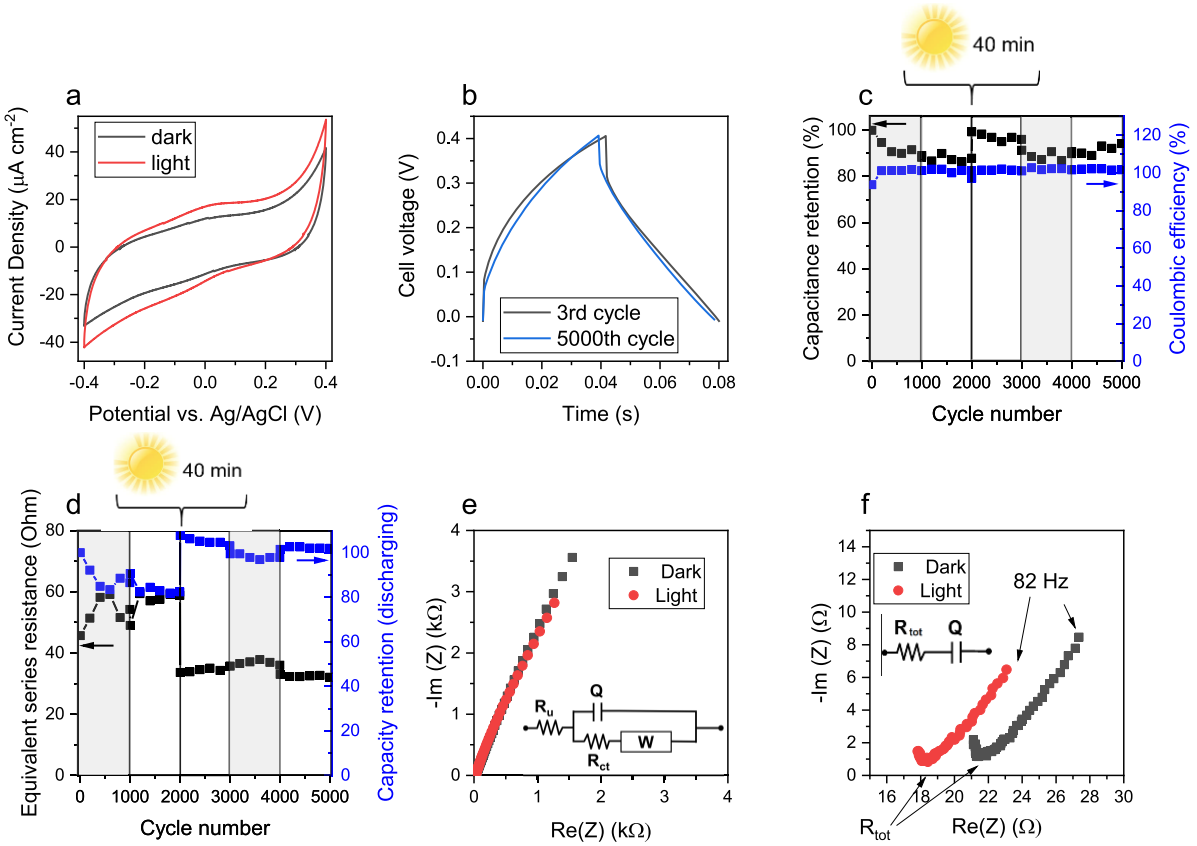

Figure 2. Electrochemical characterization of DHI-melanin in the aqueous buffer of 0.25 M $NaCH_3COO$ (pH 5) in both dark and light conditions. (a) Cyclic voltammetry at the scan rate of 5 mV s^{-1}. (b) Galvanostatic charge and discharge of the DHI-melanin supercapacitor at 5 A g^{-1}. (c) Capacitance rated to the initial value and Coulombic efficiency for 5000 cycles of galvanostatic charge and discharge. (d) Equivalent series resistance and capacity rated to the initial value for 5000 cycles of galvanostatic charge and discharge. Protocol of acquisition: dark → light → 40 min irradiation (without current or electrochemical potential applied) → light → dark → light, each for 1000 cycles. Gray rectangles indicate the dark conditions. (e) Nyquist plot in the frequency range 10^5 and 10^{-1} Hz. Inset: corresponding equivalent circuit. (f) Zoomed Nyquist plot in the frequency range 10^5−82 Hz. Inset: corresponding simplified simulated circuit. Cyclic voltammetry and electrochemical impedance experiments are performed in a three-electrode cell (i.e., they describe the single-electrode behavior), whereas galvanostatic charge and discharge characterizations refer to the full supercapacitor cell (two electrodes) (Scheme S1).

microscopy (SEM) was used to gain insight into the morphology of our samples. Cyclic voltammetry was initially performed in dark and light conditions. Afterward, we assembled the supercapacitors and characterized their electrochemical behavior. Electrochemical impedance spectroscopy was used to shed light on the working principle of the devices.

2. RESULTS AND DISCUSSION

The optical absorption spectra of DHI- and DHI/DHICA-melanins show a broadband absorption (Figure 1). Such type of absorption has been explained by different models, such as the chemical disorder model, which considers the absorption of eumelanin as the convolution of the absorption of chemically different chromophores coexisting in eumelanin, and the geometric disorder model, which considers excitonic couplings between different $\pi-\pi$ stacked oligomers.[30,31]

SEM images show that DHI- and DHI/DHICA-melanins are immobilized on the networked structure of the high-surface area carbon current collectors (Figure 1c and 1d). DHI-melanin seems to be preferentially located on flat regions between the carbon fibers. On the other hand, DHI/DHICA-melanin is preferentially located between parallel fibers.

After the characterization of the optical properties of DHI- and DHI/DHICA-melanins, we proceeded to their voltammetric investigation in a suitable aqueous electrolyte, under dark and light conditions (Figures 2a, 3a, S1, and S2). Considering the favorable proton transport properties of eumelanin, acidic electrolytes were considered.[34] Broad redox features, slightly more pronounced under light irradiation, are observable at 0.05 and −0.1 V vs Ag/AgCl. Apart from such broad features, the voltammograms are characterized by a quasi-box-shape typical of pseudocapacitive materials. With respect to electrical double-layer supercapacitors, e.g., based on bare carbon that stores energy by an electrostatic process, redox-active (pseudocapacitive) materials permit to achieve higher capacitances due to their higher charge storage capacity, related to Faradic processes.[35] Light enhances the current of the quasi-box-shaped voltammograms of melanin on carbon paper, suggesting the presence of photoenhanced (pseudo)-capacitive behavior (Figures 2a, 3a, S1, and S2). The capacity, as deduced by cyclic voltammetry, increases by ca 22% (from 2.3 to 2.8 mC cm^{-2}) for DHI-melanin and by 17% (from 1.8 to 2.1 mC cm^{-2}) for DHI/DHICA-melanin. On the other hand, the capacitance (deduced by cyclic voltammetry) increases by ca 39% (from 3.8 to 5.3 mF cm^{-2}) for DHI-melanin and by 26% (from 3.1 to 3.9 mF cm^{-2}) for DHI/DHICA-melanin (Table S2). Bare carbon paper does not

DOI: 10.1021/acsomega.9b01039
ACS Omega 2019, 4, 12244−12251

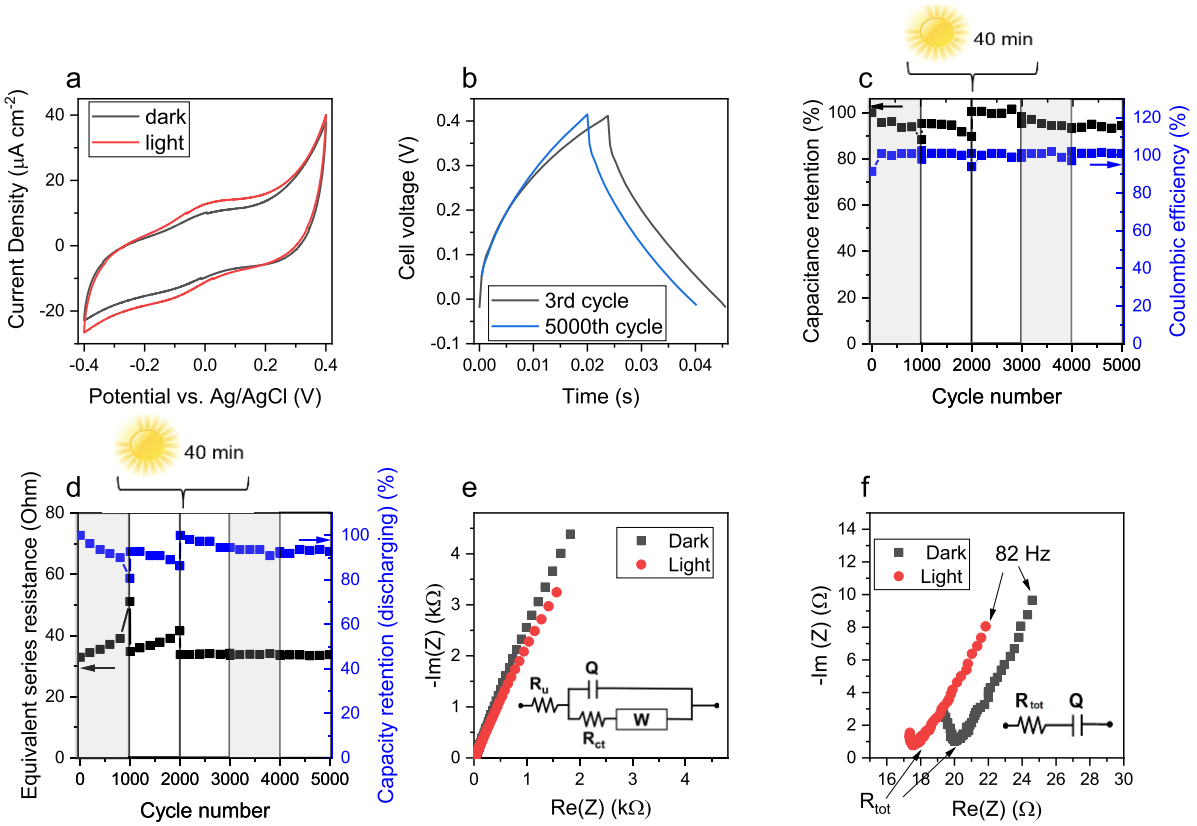

Figure 3. Electrochemical characterization of DHI/DHICA-melanin in the aqueous buffer of 0.25 M $NaCH_3COO$ (pH 5) in both dark and light conditions. (a) Cyclic voltammetry at the scan rate of 5 mV s^{-1}. (b) Galvanostatic charge and discharge curves of the DHI/DHICA-melanin supercapacitor at 5 A g^{-1}. (c) Capacitance rated to the initial value and Coulombic efficiency for 5000 cycles of galvanostatic charge and discharge. (d) Equivalent series resistance and capacity rated to the initial value for 5000 cycles of galvanostatic charge and discharge. Protocol of acquisition: dark → light → 40 min irradiation (without current or electrochemical potential applied) → light → dark → light, each for 1000 cycles. Gray rectangles indicate the dark conditions. (e) Nyquist plot in the frequency range 10^5−10^{-1} Hz. Inset: corresponding equivalent circuit. (f) Zoomed Nyquist plot in the frequency range 10^5−82 Hz. Inset: corresponding simplified simulated circuit. Cyclic voltammetry and electrochemical impedance experiments are performed in a three-electrode cell, whereas galvanostatic charge and discharge characterizations refer to the full supercapacitor cell (two electrodes) (Scheme S1).

contribute significantly to the overall current under dark and light conditions (Figure S4).

Based on the promising voltammetric results, in terms of photoresponse and stability (Figures S1 and S2), we assembled two melanin electrodes into a symmetric supercapacitor configuration and proceeded to device characterization. Galvanostatic charge and discharge measurements were conducted adopting the following protocol: dark (1000 cycles) → light (1000 cycles) → 40 min irradiation (without current or potential applied) → light (1000 cycles) → dark (1000 cycles) → light (1000 cycles), with the positive electrode facing the light source (Scheme S1). Figures 2b and 3b show a nearly triangular shape of the galvanostatic charging−discharging curves, obtained at a current density of 5 A/g (Figure S5). The quasi-linear dependence of the charge stored vs potential further supports our claim about the pseudocapacitive behavior of melanin.[36]

The small voltage drop at the beginning of the discharge (ΔV, ca 68 mV under light conditions, for both melanins) indicates the low equivalent series resistance, ESR $\left(\mathrm{ESR} = \frac{\Delta V}{2I_{dis}}\right)$, where I_{dis} is the constant (discharging) current. The supercapacitor capacitance C_{SC} $\left(C_{SC} = \frac{I_{dis}}{s}\right)$, where s is the slope of the cell voltage over time during discharge; the Coulombic efficiency η $\left(\eta = \frac{I_{dis}\, t_{dis}}{I_{ch} t_{ch}}\right)$, where t_{ch} is the charging time, I_{ch} is the constant charging current, and t_{dis} is the discharging time; the maximum power density P_{max} $\left(P_{max} = \frac{V_{max}^2}{4\ \mathrm{ESR}\ w_{sc}}\right)$, where V_{max} is the operating voltage (upper limit of the potential while charging, or cutoff potential) and w_{sc} is the loading of the active material; and the maximum energy density E_{max} $\left(E_{max} = \frac{1}{2\ w_{sc}} C_{sc} V_{max}^2\right)$ were then calculated for different experimental conditions.[37]

Figures 2c and 3c show Coulombic efficiencies of ca 100% through 5000 cycles for both DHI- and DHI/DHICA-melanins. After 3000 cycles and 40 min of light irradiation, the capacitance of our two melanins, rated to the initial values, increases to a value of ca 96% from a value of 88% observed after 1000 cycles in the dark (Figures 2c and 3c). At the same time, the capacity rated to the initial value increases from ca 86 to ca 103% for DHI-melanin and from ca 80 to ca 94% for DHI/DHICA-melanin (Figures 2d and 3d, and Tables S3 and S4). The values of the ESR are significantly stable after 40 min of continuous irradiation (Figures 2d and 3d).

Comparing the average values calculated for the range of cycles 1001−2000 and 2001−3000, including 40 min of irradiation between the two ranges of cycles, the power density

DOI: 10.1021/acsomega.9b01039
ACS Omega 2019, 4, 12244−12251

increases by ca 56% (from 3.8 to 5.9 W g^{-1}) and the energy density by 18% (from 44 to 52 mJ g^{-1}, i.e., from 0.0122 to 0.0144 mWh g^{-1}), for DHI-melanin. In other words, the irradiation of the samples in the absence of applied electrochemical potential increases the power density and energy density of the device. Analogously, for DHI/DHICA-melanin, the power density increases by 12% (from 5.3 to 5.9 W g^{-1}) and the energy density by 6% (from 27 to 28 mJ g^{-1}, i.e., from 0.0075 to 0.0078 mWh g^{-1}).

To study the pseudocapacitive behavior of melanins under light conditions, we carried out electrochemical impedance spectroscopy measurements.[38] Nyquist plots of both melanin electrodes (Figures 2e, 3e, and S3) show a pseudocapacitive behavior for both dark and light conditions, modeled by the equivalent circuit reported in the inset of Figures 2e and 3e. R_u is the uncompensated resistance that includes the electronic resistance of the electrodes and the ionic resistance of the electrolyte. R_u is affected by the cell geometry (i.e., by the distance between the working and reference electrodes). R_u is in series with the charge-transfer resistance, R_{ct}, which describes the kinetics of the electron-transfer processes, namely, the Faradic reactions taking place at melanin. Pseudocapacitive processes, such Faradic reactions, give rise to a capacitive response that is modeled with the constant phase element Q, in parallel with R_{ct}, to take into account any deviation from an ideal capacitive response. The impedance of Q is $Z_Q = (1/Q)(j\omega)^{-n}$, with ω being the frequency; it corresponds to that of a pure capacitor when $n = 1$. For $n = 1$, the imaginary impedance $\mathrm{Im}(Z)$ relates to the capacitance as for the following equation: $\mathrm{Im}(Z) = j/(\omega C)$. The ($R_{ct}$ Q) parallel elements describe the high-frequency semicircle (that is only partial due to the selected frequency range; Figures 2f and 3f). The diameter of the semicircles corresponds to R_{ct}. The equivalent circuit also includes a Warburg element (W), which describes any process controlled by diffusion (ion diffusion through the melanin on carbon paper but also diffusion of electrons through melanin). The Nyquist plots indicate that, for both melanins electrodes, light has an effect on the electrode impedance. Indeed, the high-frequency resistances shift toward lower values under light exposure, thereby suggesting that the electronic resistances, that contribute to R_u and R_{ct}, decrease too. Simultaneously, the low-frequency $\mathrm{Im}(Z)$ decreases, implying that the capacitance increases. Bare carbon paper has almost the same resistance under light and dark conditions (Figure S4). These observations support the hypothesis that the Faradic reactions that drive the pseudocapacitive response of melanin electrodes are promoted by light illumination. It is not possible to separately fit the high-frequency semicircle to get R_{ct} (the semicircle is not complete because only a few points are available in the corresponding frequency range). Therefore, to better quantify the impedance changes under light and dark conditions, we fitted the low-frequency linear plots (2 kHz to 82 Hz region) with a simplified circuit R_{tot} Q (Figures 2f and 3f), where R_{tot} includes the uncompensated and charge-transfer resistance, i.e., $R_{tot} = R_u + R_{ct}$, and is in series with Q, the capacitive element. Importantly, the fitting procedure indicates a 15% decrease in R_{tot} for DHI-melanin and a 11% decrease in DHI/DHICA-melanin after light exposure (Table S5).

We explain the increased responses of DHI- and DHI/DHICA-melanins under irradiation conditions by the action of the light that increases the number of charge carriers stored in the melanin (Scheme 2). In the dark, the positively biased

Scheme 2. Light-Assisted Melanin-Based Supercapacitor Investigated in This Work

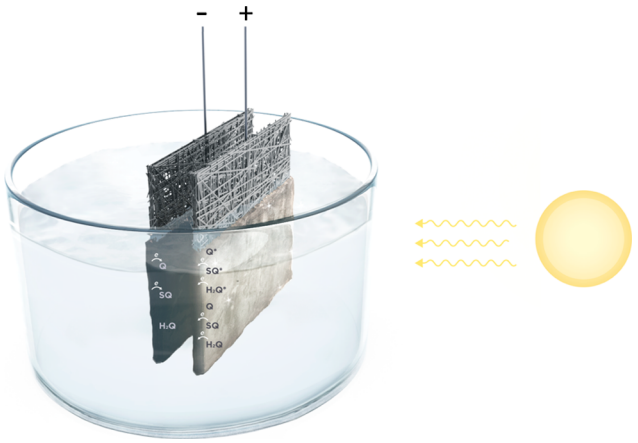

melanin electrode (with redox species largely present in the SQ and Q redox forms) experiences electron transfers from SQ to the carbon paper to produce Q. When light is absorbed by melanin, it excites electrons from the ground electronic state to the excited state, from where electrons are easily transferred to the carbon paper. Therefore, the total capacity of melanin is enhanced under irradiation by the higher number of electron-transfer events due to photoinduced transfers from excited states taking place in parallel to the transfers due to applied electrochemical potential. In other words, the observed increase of melanin capacity under illumination can be explained with the enhancement of the kinetics, under light conditions, of the Faradic reactions that drive the pseudocapacitive response of the melanin electrodes. This enhancement of the kinetics brings about higher charge accumulation at the Inner Helmotz Plane (IHP) and consequently higher C_{IHP} (IHP capacitance). On the negatively biased electrode, SQ is the redox state of melanin expected mainly to accept electrons (H2Q is already in the reduced form, and Q is expected to have been already reduced because of the electrochemical potential applied). Furthermore, the light-induced increase of the charge-carrier density in melanin on carbon electrodes is expected to improve the capacitive contribution of the solid component (namely melanin on carbon) of the electrode/electrolyte interface, leading to the improvement of the overall capacitance.[36]

3. CONCLUSIONS

We reported on the use of chemically controlled melanins (DHI- and DHI/DHICA-melanins) processed by a simple, environmentally friendly method as sustainable organic redox materials for light-assisted (pseudo)supercapacitors where the storage performance of the device is improved under solar light. The broadband absorption and the redox properties of the natural biopigment melanin inspired us to explore the possibility to enhance the storage properties of melanin electrodes under solar light. We observed that the solar light improves the capacitance, capacity, stability, and decreases the resistance of the melanin electrodes. Coulombic efficiencies of ca 100%, during 5000 cycles, were observed. After 3000 cycles and 40 min light irradiation, the capacitance and capacity of our melanin electrodes, rated to the initial value, improved significantly. Despite the fact that the electrode capacitance is low compared to that of commercial supercapacitors, these

DOI: 10.1021/acsomega.9b01039
ACS Omega 2019, 4, 12244−12251

findings are of interest for microenergy-storage applications, like those required for wearable and implantable devices. Comparing the average values calculated for the range of cycles 1001−2000 and 2001−3000, including 40 min of irradiation between the two ranges of cycles, the maximum power density increased by ca 56% (from 3.8 to 5.9 W g^{-1}), whereas the maximum energy density increased by 18% (from 44 to 52 mJ g^{-1}) for DHI-melanin. In other words, the irradiation of the samples, in the absence of applied electrochemical potential, enhances the power and energy density of the devices. This points to the remarkable operational robustness of our organic electrodes under illumination conditions. When comparing the performance of DHI- and DHI/DHICA-melanins, we observe that DHI-melanin features superior storage performance. Among others, such an observation points to the role of the melanin structure on the electrochemical energy storage properties: the structure of DHI-melanin is characterized by an ordered $\pi-\pi$ stacking expected to promote efficient electronic transport, which is beneficial to the overall storage performance. In agreement with that, the relatively disordered structure of DHI/DHICA-melanin is expected to lead to poorer performance.[24]

Other organic materials extracted from natural sources featuring biodegradability are currently investigated by our research groups for their light-assisted energy-storage performance to demonstrate the universality of the organic solar electrochemical energy storage concept. The outcomes of our research impact a broad range of fields, from environmentally benign energy technologies that avoid toxic, critical, and expensive materials to biocompatible powering elements and autonomous wearable devices.

4. EXPERIMENTAL SECTION

4.1. Preparation of DHI- and DHI/DHICA-Melanins on Carbon Paper. Chemically controlled eumelanins, i.e., DHI-melanin and (7/3 weight/weight) DHI/DHICA-melanin, were synthesized in situ on carbon paper by a solid-state polymerization method already reported in the literature.[39,40] Ten milligram per milliliter solution of DHI was prepared in ambient conditions and used as a precursor. For DHI/DHICA-melanin, 10 mg of powder, including 7 mg of DHI monomer powder and 3 mg of DHICA monomer powder, was dissolved in methanol in ambient conditions, and the solution was used as a precursor. Afterward, the monomer solution (10 μL) was drop-cast on the carbon paper (Spectracarb 2050A, 10 mils, geometric area 1.0 cm^2). The loading of melanin on each carbon paper current collector was ca 0.1 mg cm^{-2}. After drop-casting, the samples were exposed to NH_3 vapors from $NH_{3(aq)}$ (Sigma-Aldrich, 28−30% w/v) for about 68 h to catalyze the polymerization reaction.

4.2. Preparation of the Electrolytes. Buffer solutions of $NaCH_3COO$, 0.25 M and pH ca 5, were prepared from $NaCH_3COO$ (Sigma-Aldrich >99%) and CH_3COOH (Sigma-Aldrich >99.7%) dissolved in deionized water (18.2 MΩ cm).

4.3. Electrochemical Measurements. Electrochemical measurements were performed using a Biologic bipotentiostat (SP-300) in a three-electrode cell, with carbon paper current collectors loaded with melanin as the working electrode, a Pt mesh as the counter electrode, and $Ag/AgCl_{(aq)}$ in 1 M KCl as the reference electrode. For galvanostatic measurements, two identical melanin-on-carbon-paper electrodes were employed as working and counter electrodes and $Ag/AgCl_{(aq)}$ in 1 M KCl as the reference electrode to monitor each electrode behavior during the tests. A solar simulator (SLB300A, Sciencetech) was used for electrochemical experiments under light conditions (1 Sun).

Cyclic voltammetry was performed in the potential range −0.4 V/0.4 V vs $Ag/AgCl_{(aq)}$ at 5 mV s^{-1} adopting the following sequence: dark (6 cycles) → light (16 cycles) → dark (14 cycle). After that, electrochemical impedance spectroscopy (EIS) measurements were conducted in a three-electrode setup, within the frequency range of 10^5−10^{-1} Hz, adopting the sequence EIS (dark) → 40 min irradiation (without electrochemical potential applied) → EIS (light). With the same sequence and setup, another set of EIS measurements were conducted, at open-circuit potentials (OCP), within the frequency range of 10^6−10^{-1} Hz, adopting the sequence: OCP vs time (dark) → EIS (dark) → 40 min irradiation (without electrochemical potential applied) → OCP vs time (light) → EIS (light). Two identical electrodes were precycled (5 cycles) in the potential range −0.6 V/0.6 V vs $Ag/AgCl_{(aq)}$ at 5 mV s^{-1}, and then galvanostatic charge−discharge characterizations under dark and light conditions were performed in supercapacitor symmetric configuration, with 1 mm interelectrode distance (to avoid possible heating effects on the device performance). Five thousand cycles of galvanostatic charge−discharge were performed, with a current density of 5 A g^{-1} and a cutoff potential of 0.4 V. An Ag/AgCl reference electrode was used to monitor the potential of the positive and negative electrodes during the galvanostatic charge/discharge.

We monitored the temperature of the cell using two experimental configurations: a thermocouple attached to the outer wall of the electrochemical cell and a thermometer immersed in the cell. The cell, during the temperature measurements, contained $NaCH_3COO$ buffer aqueous solution (pH 5) and three electrodes (cyclic voltammetry configuration, without nitrogen purging). The temperature was monitored for ca 2 h, every 5−10 min. The results of the measurements indicate that the temperature change was ≤3.5 °C during light irradiation.

4.4. Morphology. The morphology of the melanin on carbon electrodes was examined by scanning electron microscopy (SEM, JEOL JSM7600F) at an acceleration voltage of 5 kV in backscattered electron (BSE) imaging mode. The melanin on carbon electrodes were stained with uranyl acetate for 1 h prior to morphology examination by SEM.[25,26,32,33]

4.5. Optical Characterization. The UV−vis spectra of DHI- and DHI/DHICA-melanin samples, spin-coated (30 s at 2000 rpm, 10 mg mL^{-1} solution) on Corning glass (pre-cleaned 25 mm × 20 mm, thickness 0.96−1.06 mm), were acquired by a PerkinElmer LAMBDA 1050 spectrophotometer equipped with a Labsphere integrating sphere, allowing for the total reflected R and transmitted T radiation to be measured simultaneously and obtaining the resulting absorption of the films by posing $A = 1 - (R + T)$.

■ ASSOCIATED CONTENT

Supporting Information

The Supporting Information is available free of charge on the ACS Publications website at DOI: 10.1021/acsomega.9b01039.

Cycling stability of melanin electrodes, transient characteristics, electrochemical impedance spectroscopy,

DOI: 10.1021/acsomega.9b01039
ACS Omega 2019, 4, 12244−12251

galvanostatic measurements, and tables including literature review and capacitance and capacity values (PDF)

AUTHOR INFORMATION

Corresponding Authors

*E-mails: francesca.soavi@unibo.it (F.S.).
*E-mails: clara.santato@polymtl.ca (C.S.).

ORCID

Francesca Soavi: 0000-0003-3415-6938
Clara Santato: 0000-0001-6731-0538

Author Contributions

‖R.X. and A.G. contributed equally to this work.

Notes

The authors declare no competing financial interest.

ACKNOWLEDGMENTS

Y. Drolet and J. Bouchard are acknowledged for technical support. A.G. is grateful to the Institut de l'Énergie Trottier for financial support through a Ph.D. scholarship. C.S. and F.S. acknowledge the Bilateral Italy−Quebec Mobility program 2017−2019 (MRIF) for financial support. C.S. is grateful to NSERC (Discovery) and FQRNT (Équipe) for financial support.

REFERENCES

(1) International Energy Agency. *World Energy Outlook 2017*, 2017.
(2) Armaroli, N.; Balzani, V. *Powering Planet Earth: Energy Solutions for the Future*; John Wiley & Sons: New York City, 2012.
(3) Arico, A. S.; Bruce, P.; Scrosati, B.; Tarascon, J. M.; Van Schalkwijk, W. Nanostructured Materials for Advanced Energy Conversion and Storage Devices. In *Materials For Sustainable Energy: A Collection of Peer-Reviewed Research and Review Articles from Nature Publishing Group*; World Scientific: Singapore, Singapore, 2011; pp 148−159.
(4) Vlachopoulos, N.; Hagfeldt, A. Photobatteries and Photocapacitors. In *Molecular Devices for Solar Energy Conversion and Storage*; Springer: New York, 2018; pp 281−325.
(5) Zhou, Y.; Wang, B.; Liu, C.; Han, N.; Xu, X.; Zhao, F.; Fan, J.; Li, Y. Polyanthraquinone-Based Nanostructured Electrode Material Capable of High-Performance Pseudocapacitive Energy Storage in Aprotic Electrolyte. *Nano Energy* **2015**, *15*, 654−661.
(6) Song, Z.; Qian, Y.; Liu, X.; Zhang, T.; Zhu, Y.; Yu, H.; Otani, M.; Zhou, H. A Quinone-Based Oligomeric Lithium Salt for Superior Li-Organic Batteries. *Energy Environ. Sci.* **2014**, *7*, 4077−4086.
(7) Kim, Y. J.; Wu, W.; Chun, S.-E.; Whitacre, J. F.; Bettinger, C. J. Biologically Derived Melanin Electrodes in Aqueous Sodium-Ion Energy Storage Devices. *Proc. Natl. Acad. Sci. U.S.A.* **2013**, *110*, 20912−20917.
(8) Liang, Y.; Tao, Z.; Chen, J. Organic Electrode Materials for Rechargeable Lithium Batteries. *Adv. Energy Mater.* **2012**, *2*, 742−769.
(9) Wang, C.; Yang, Z.; Wang, Y.; Zhao, P.; Yan, W.; Zhu, G.; Ma, L.; Yu, B.; Wang, L.; Li, G.; et al. High-Performance Alkaline Organic Redox Flow Batteries Based on 2-Hydroxy-3-Carboxy-1,4-Naphthoquinone. *ACS Energy Lett.* **2018**, *3*, 2404−2409.
(10) Hardee, D.; Chen, Q.; Gordon, R. G.; Kim, S. B.; Marshak, M. P.; Tong, L.; Aziz, M. J.; Eisenach, L.; Lin, K.; Valle, A. W.; et al. Alkaline Quinone Flow Battery. *Science* **2015**, *349*, 1529−1532.
(11) Gao, C.; Zhao, L.; Wang, M. Stabilization of a Reactive Polynuclear Silver Carbide Cluster through the Encapsulation within a Supramolecular Cage. *J. Am. Chem. Soc.* **2012**, *134*, 824−827.
(12) Liang, Y.; Jing, Y.; Gheytani, S.; Lee, K.; Liu, P.; Facchetti, A.; Yao, Y. Universal Quinone Electrodes for Long Cycle Life Aqueous Rechargeable Batteries. *Nat. Mater.* **2017**, *16*, 841−850.
(13) Janoschka, T.; Martin, N.; Martin, U.; Friebe, C.; Morgenstern, S.; Hiller, H.; Hager, M. D.; Schubert, U. S. An Aqueous, Polymer-Based Redox-Flow Battery Using Non-Corrosive, Safe, and Low-Cost Materials. *Nature* **2015**, *527*, 78−81.
(14) Gerhardt, M. R.; Galvin, C. J.; Huskinson, B.; Marshak, M. P.; Suh, C.; Chen, X. A Metal-Free Organic-Inorganic Aqueous Flow Battery. *Nature* **2014**, *505*, 195−198.
(15) Naoi, K.; Suematsu, S.; Hanada, M.; Takenouchi, H. Enhanced Cyclability of π-π Stacked Supramolecular (1,5-Diaminoanthraquinone) Oligomer as an Electrochemical Capacitor Material. *J. Electrochem. Soc.* **2002**, *149*, A472−A477.
(16) Sun, T.; Li, Z.; Wang, H.; Bao, D.; Meng, F.; Zhang, X. A Biodegradable Polydopamine-Derived Electrode Material for High-Capacity and Long-Life Lithium-Ion and Sodium-Ion Batteries. *Angew. Chem.* **2016**, *128*, 10820−10824.
(17) Song, Z.; Zhou, H. Towards Sustainable and Versatile Energy Storage Devices: An Overview of Organic Electrode Materials. *Energy Environ. Sci.* **2013**, *6*, 2280−2301.
(18) Mukhopadhyay, A.; Jiao, Y.; Katahira, R.; Ciesielski, P. N.; Himmel, M.; Zhu, H. Heavy Metal-Free Tannin from Bark for Sustainable Energy Storage. *Nano Lett.* **2017**, *17*, 7897−7907.
(19) Vonlanthen, D.; Lazarev, P.; See, K. A.; Wudl, F.; Heeger, A. J. A Stable Polyaniline-Benzoquinone-Hydroquinone Supercapacitor. *Adv. Mater.* **2014**, *26*, 5095−5100.
(20) Di Mauro, E.; Xu, R.; Soliveri, G.; Santato, C. Natural Melanin Pigments and Their Interfaces with Metal Ions and Oxides: Emerging Concepts and Technologies. *MRS Commun.* **2017**, *7*, 141−151.
(21) Jastrzebska, M.; Kocot, A.; Tajber, L. Photoconductivity of Synthetic Dopa-Melanin Polymer. *J. Photochem. Photobiol., B* **2002**, *66*, 201−206.
(22) Meredith, P.; Bettinger, C. J.; Irimia-Vladu, M.; Mostert, A. B.; Schwenn, P. E. Electronic and Optoelectronic Materials and Devices Inspired by Nature. *Rep. Prog. Phys.* **2013**, *76*, No. 034501.
(23) Pezzella, A.; D'Ischia, M.; Napolitano, A.; Palumbo, A.; Prota, G. An Integrated Approach to the Structure of Sepia Melanin. Evidence for a High Proportion of Degraded 5, 6-Dihydroxyindole-2-Carboxylic Acid Units in the Pigment Backbone. *Tetrahedron* **1997**, *53*, 8281−8286.
(24) Panzella, L.; Gentile, G.; D'Errico, G.; Della Vecchia, N. F.; Errico, M. E.; Napolitano, A.; Carfagna, C.; D'Ischia, M. Atypical Structural and π-Electron Features of a Melanin Polymer That Lead to Superior Free-Radical-Scavenging Properties. *Angew. Chem., Int. Ed.* **2013**, *52*, 12684−12687.
(25) Xu, R.; Prontera, C. T.; Di Mauro, E.; Pezzella, A.; Soavi, F.; Santato, C. An Electrochemical Study of Natural and Chemically Controlled Eumelanin. *APL Mater.* **2017**, *5*, No. 126108.
(26) Kumar, P.; Di Mauro, E.; Zhang, S.; Pezzella, A.; Soavi, F.; Santato, C.; Cicoira, F. Melanin-Based Flexible Supercapacitors. *J. Mater. Chem. C* **2016**, *4*, 9516−9525.
(27) Kim, Y. J.; Wu, W.; Chun, S. E.; Whitacre, J. F.; Bettinger, C. J. Catechol-Mediated Reversible Binding of Multivalent Cations in Eumelanin Half-Cells. *Adv. Mater.* **2014**, *26*, 6572−6579.
(28) Mula, G.; Manca, L.; Setzu, S.; Pezzella, A. Photovoltaic Properties of PSi Impregnated with Eumelanin. *Nanoscale Res. Lett.* **2012**, *7*, 1−21.
(29) Antidormi, A.; Melis, C.; Canadell, E.; Colombo, L. Assessing the Performance of Eumelanin/Si Interface for Photovoltaic Applications. *J. Phys. Chem. C* **2017**, *121*, 11576−11584.
(30) Tran, M. L.; Powell, B. J.; Meredith, P. Chemical and Structural Disorder in Eumelanins - A Possible Explanation for Broad Band Absorbance. *Biophys. J.* **2006**, *90*, 28.
(31) Chen, C.; Chuang, C.; Cao, J.; Ball, V.; Ruch, D.; Buehler, M. J. Excitonic Effects from Geometric Order and Disorder Explain Broadband Optical Absorption in Eumelanin. *Nat. Commun.* **2014**, *5*, No. 3859.
(32) Hong, L.; Simon, J. D. Current Understanding of the Binding Sites, Capacity, Affinity, and Biological Significance of Metals in Melanin. *J. Phys. Chem. B* **2007**, *111*, 7938−7947.

DOI: 10.1021/acsomega.9b01039
ACS Omega 2019, 4, 12244−12251

(33) Sakaguchi, T.; Nakajima, A. Accumulation of Uranium by Biopigments. *J. Chem. Technol. Biotechnol.* **1987**, *40*, 133−141.
(34) Wünsche, J.; Deng, Y.; Kumar, P.; Di Mauro, E.; Josberger, E.; Sayago, J.; Pezzella, A.; Soavi, F.; Cicoira, F.; Rolandi, M.; et al. Protonic and Electronic Transport in Hydrated Thin Films of the Pigment Eumelanin. *Chem. Mater.* **2015**, *27*, 436−442.
(35) Brousse, T.; Bélanger, D.; Long, J. W. To Be or Not To Be Pseudocapacitive? *J. Electrochem. Soc.* **2015**, *162*, A5185−A5189.
(36) Bard, A. J.; Faulkner, L. R. *Electrochemical Methods: Fundamentals and Applications*, 2nd ed.; John Wiley & Sons: New York City, 2000.
(37) Zhang, S.; Pan, N. Supercapacitors Performance Evaluation. *Adv. Energy Mater.* **2015**, *5*, No. 1401401.
(38) Orazem, M. E.; Tribollet, B. *Electrochemical Impedance Spectroscopy*; John Wiley & Sons: New York City, 2011.
(39) Pezzella, A.; Barra, M.; Musto, A.; Navarra, A.; Alfè, M.; Manini, P.; Parisi, S.; Cassinese, A.; Criscuolo, V.; D'Ischia, M. Stem Cell-Compatible Eumelanin Biointerface Fabricated by Chemically Controlled Solid State Polymerization. *Mater. Horiz.* **2015**, *2*, 212−220.
(40) D'Ischia, M.; Napolitano, A.; Pezzella, A.; Land, E. J.; Ramsden, C. A.; Riley, P. A. 5,6-Dihydroxyindoles and Indole-5,6-Diones. *Adv. Heterocycl. Chem.* **2005**, *89*, 1−63.

DOI: 10.1021/acsomega.9b01039
ACS Omega 2019, 4, 12244−12251